IOP PUBLISHING MODELLING AND SIMULATION IN MATERIALS SCIENCE AND ENGINEERING

Modelling Simul. Mater. Sci. Eng. **16** (2008) 085005 (12pp) doi:10.1088/0965-0393/16/8/085005

Comparison of thermal properties predicted by interatomic potential models

Seunghwa Ryu[1] **and Wei Cai**[2]

[1] Department of Physics, Stanford University, CA 94305, USA
[2] Department of Mechanical Engineering, Stanford University, CA 94305, USA

E-mail: shryu@stanford.edu and caiwei@stanford.edu

Received 29 May 2008, in final form 12 August 2008
Published 1 October 2008
Online at stacks.iop.org/MSMSE/16/085005

Abstract

We report melting points and other thermal properties of several semiconducting and metallic elements as they are modeled by different empirical interatomic potential models, including the Stillinger–Weber, the embedded-atom method, the Finnis–Sinclair and the modified-embedded-atom method. The state-of-the-art free energy methods are used to determine the melting points of these models within a very small error bar, so that they can be cross-compared with each other. The comparison reveals several systematic trends among elements with the same crystal structure. It identifies areas that require caution in the application of these models and suggests directions for their future improvement.

1. Introduction

Empirical or semi-empirical potential models play an important role in computational materials science because many interesting processes involve the collective dynamics of thousands of atoms, which is still too expensive for *ab initio* models. At the same time, due to their (semi-) empirical nature, the potential models need to be thoroughly benchmarked before they can be trusted to make reliable, new, predictions. The structural and mechanical properties of a single phase (liquid or solid) have been extensively studied by computer simulations based on empirical potentials with considerable success. There is a growing interest in applying these models to study more complex processes, such as the catalytic growth of a silicon nanowire from a eutectic liquid droplet, which involves the transformation between different phases. For these applications, it is very important for the potential models to provide a reasonable description of the melting point and other thermal properties. But the empirical potential models have not been extensively tested for these properties, mostly due to the difficulty in accurately determining the melting point.

Generally speaking, there are two ways to compute the melting point of a crystal from atomistic simulation. In the 'co-existence method', the liquid and solid co-exist with an interface in the simulation cell. The melting temperature is determined by finding the temperature at which both the liquid and the solid phases are stable. While this method is easy to set up, fluctuations in the instantaneous temperature and the slow kinetics of solid–liquid interface motion introduce statistical and systematic errors in the estimation of the melting point [1, 2]. In the 'free energy' method, the Gibbs free energies of the solid and liquid phases are computed as functions of temperature, and the melting point is determined by their intersection point. The free energy method has been applied to determine the melting point of the Stillinger–Weber (SW) model of silicon as early as 1987 [3]. Since then, several advanced free energy methods have been developed which make free energy and melting point calculations more efficient [4, 5], and many of them have been applied in melting point calculations [6]. While the free energy method is more difficult to set up, we find that it is more efficient than the interface method if we need to determine the melting point within a very small error bar, e.g. ± 1 K. The difficulty in setting up the various free energy calculations necessary for the determination of melting points is removed by the development of an automatic computer script [7].

In this paper, we show that accurate melting points can be obtained from the state-of-the-art free energy methods. For the first time, we present a systematic comparison of the melting points, latent heat, entropy and thermal expansion coefficients of nine representative elements described by four different potential models, including SW [8, 9], the embedded-atom-method (EAM) [10, 11], Finnis–Sinclair (FS) [12] and the modified-embedded-atom-method (MEAM) [13]. The comparison in this work identifies areas that require caution in the application of these potential models and also suggests directions for their future improvement. Before we begin, we shall briefly describe the differences and relationship among these potential models [22]. All four models are many-body potentials, i.e. they contain terms that cannot be written as a sum over pairs of atoms. In the SW potential, a sum of three-body terms is introduced specifically to stabilize the tetrahedral bond angle in the diamond-cubic crystal structure. Hence the SW potential is designed for semiconducting crystals and is called a three-body potential. The other three models are called many-body potentials because the potential energy cannot be written as a sum of two-body and three-body terms. The EAM model is designed to capture the many-body effect in metals, in which the electrons are more diffuse and shared by more atoms than the electrons in semiconductors. For each atom, the EAM potential contains an embedding function that describes the energy to embed this atom into the electron background generated by its neighbors. The EAM model is widely used to describe face-centered-cubic (FCC) metals. The FS model can be regarded as a special type of EAM model, with its specific choice of the embedding function, and is a commonly used model for body-centered-cubic (BCC) metals. The goal of the MEAM model was to combine the angular dependence of covalent bonds and the many-body effect for metallic bonds within a unified scheme, in order to provide a basis for modeling systems (e.g. Si–Au) where both types of bonding may exist. As a generalization to the EAM model, the embedding energy in the MEAM model depends not only on the total electron density contributed by neighboring atoms but also on their angular distribution.

The paper is organized as follows. In section 2, we present the comparison between the predictions from different potential models with experiments. In section 3, we describe the important details in our free energy calculations for the accurate determination of melting points. We organize the paper in this way because we think the results themselves, compared with the computational methods that enabled such calculations, should be of interest to a wider audience. A brief summary and outlook for the future research is given in section 4.

Table 1. Thermal properties of various elements as predicted by several empirical potentials and compared with experiments [14–16]. The properties include the melting point T_m (K), latent heat of fusion L (J g^{-1}), solid and liquid entropy at melting point, S_S and S_L (J mol^{-1} K^{-1}), and thermal expansion coefficient α (10^{-6} K^{-1}) at 300 K. The MEAM*-Au and MEAM*-Cu entries correspond to a modification of the original MEAM model by changing c_{min} from 2.0 to 0.8. The MEAM† entries of BCC metals are computed by the new MEAM model that includes second nearest neighbor interactions [17, 18].

	Model	T_m	L	S_S	S_L	α
Si	MEAM	1411.3 ± 0.4	1309	48.74	74.79	13.6
Si	SW	1694.7 ± 0.5	1111	58.02	76.45	3.9
Si	Exp	1687	1650	61.765	91.562	2.6
Ge	MEAM	1216.2 ± 0.6	427	58.34	83.84	16.2
Ge	SW	2898.0 ± 1.7	847	84.07	105.30	5.8
Ge	Exp	1211	465	66.77	97.34	5.8
Au	MEAM	1120.0 ± 0.6	92	77.47	93.72	2.0
Au	MEAM*	995.3 ± 1.3	52	84.18	94.47	16.5
Au	EAM	984.3 ± 2.3	41	85.73	94.03	13.5
Au	Exp	1337.3	64.9	—	—	14.2
Cu	MEAM	1350.0 ± 1.0	368	62.70	80.19	4.5
Cu	MEAM*	1182.9 ± 2.2	205	69.69	80.68	16.0
Cu	EAM	1239.6 ± 2.3	164	71.78	80.17	17.3
Cu	Exp	1357.8	205	74.30	83.97	16.5
Ag	MEAM	987.1 ± 0.9	158	66.21	83.49	5.1
Ag	Exp	1234.9	103	—	—	18.9
Pb	MEAM	674.7 ± 1.0	57	76.17	93.59	3.3
Pb	Exp	600.6	23.2	84.34	92.31	28.9
Mo	MEAM	<1000	—	—	—	8.6
Mo	MEAM†	2778.0 ± 10.1	153	91.98	97.28	5.3
Mo	FS	3062.6 ± 7.6	284	91.85	100.75	2.9
Mo	Exp	2896	290	98.10	110.52	4.8
Ta	MEAM	<1000	—	—	—	9.1
Ta	MEAM†	2884.3 ± 7.9	115	102.56	109.75	5.7
Ta	FS	3935.7 ± 6.7	190	104.8	113.54	6.3
Ta	Exp	3290	174	111.26	122.48	6.3
W	MEAM	<1000	—	—	—	6.1
W	MEAM†	4389.0 ± 9.1	161	106.24	112.98	4.2
W	FS	4125.6 ± 8.0	184	103.81	112.03	3.9
W	Exp	3695	192	108.90	118.52	4.5

2. Comparison between model predictions and experiments

Table 1 summarizes all the numerical results in this work. The melting point T_m, latent heat of fusion L, and entropy of solid and liquid at melting point, S_S and S_L and thermal expansion coefficient α are computed for nine pure elements. The elements are organized into three groups: semiconductors (Si, Ge), FCC metals (Au, Cu, Ag, Pb) and BCC metals (Mo, Ta, W). MEAM is the only model that has been fitted to elements in all three groups. SW, EAM and FS models are fitted to semiconductors, FCC metals and BCC metals, respectively. In the following we compare the predictions from different potential models with experiments in these three groups separately.

2.1. Semiconductors: Si and Ge

The melting point of Si predicted by the MEAM model is 16% (277 K) lower than the experimental value, whereas the prediction from the SW model is less than 1% away from the experimental value. But the SW model for Si is fitted to the melting point [8]. On the other hand, the SW model for Ge is not fitted to the melting point and it grossly overestimates the melting point (by more than 100%) [9]. In comparison, the MEAM prediction of Ge melting point is very accurate (less than 1%). The MEAM model also correctly predicts that Si has a higher melting point than Ge. The melting point of the SW-Si model is consistent with the earlier report of 1691 ± 20 K, also using the free energy method [3]. The melting point of the MEAM-Si model is somewhat lower than the earlier report of 1475 ± 25 K, using the co-existence method [1]. This is due to the difference in the potential models used in both studies[3].

A byproduct from the free energy calculation of the melting point is the slope of the Gibbs free energy–temperature curve at the melting temperature, for both solid and liquid phases. From these we can extract the entropy of the solid and liquid phases, S_S and S_L, at the melting point, and the latent heat of fusion from $L = T_m(S_L - S_S)$, all of which can be compared with experiments. It is interesting to note that S_S, S_L and L are underestimated by the MEAM-Si, SW-Si and MEAM-Ge models, even though SW-Si and MEAM-Ge predict melting points accurately. A similar trend was also reported in the environment-dependent interatomic potential (EDIP) of Si [6]. This implies the difficulties in describing the solid phase and liquid phase by a single empirical model due to their fundamentally different bonding mechanisms: the former is a low coordination semiconductor and the latter is an intermediate coordination metal.

A point of concern is that the MEAM potential predicts a thermal expansion coefficient (at room temperature) that is 3 to 5 times larger than experimental values. It is possible that by adding a short range potential between Si atoms, both the melting point and the thermal expansion coefficients of the MEAM-Si model may be improved [20]. This possibility will be explored in a future publication.

2.2. FCC metals: Au, Cu, Ag and Pb

The performance of the MEAM model in FCC metals is generally satisfactory. When comparison with the EAM model is available (Au and Cu), the MEAM model predicts a melting point that is closer to the experimental data. However, the MEAM model predicts a thermal expansion coefficient that is about 4 to 10 times smaller than experimental data, exactly the opposite to the case of the semiconductors.

Fortunately, by changing the angular screening factor of the MEAM potential from the default value of $c_{min} = 2.0$ to $c_{min} = 0.8$, the thermal expansion coefficient is greatly improved, as shown in the MEAM* entries in table 1. This modification also improves the accuracy of latent heat and entropies of solid and liquid. The generalized stacking fault, an important property for dislocation modeling, is also significantly improved when c_{min} is changed to 0.8 [21].

Hence we suggest that the MEAM model for FCC metals can be generally improved by reducing its angular screening parameter c_{min}. The corresponding decrease of melting point

[3] An earlier version of MEAM [19] without angular cut-off is used in Cook *et al* [1] and a later version of MEAM [13] is used in this work. We also computed the melting point of the later version of MEAM [13] using the co-existence method and the melting point is around 1410 K.

may be compensated by adding a short range potential. This hypothesis will be tested in a future publication.

2.3. BCC metals: Mo, Ta and W

MEAM and FS models are examined for three typical BCC metals (Mo, Ta, W). Because BCC metals generally have much higher melting points than semiconductors and FCC metals, the simulations here experience larger statistical fluctuations, leading to larger error bars in the predicted melting points. The FS model overestimates melting points of Mo, Ta and W by about 10–20%. The latent heat, entropy and thermal expansion coefficient are all in good agreement with experimental values. Hence the FS model describes the thermal properties of BCC metal very well.

Unfortunately, the original MEAM model seems to fail dramatically in the prediction of thermal properties of BCC metals. For all three elements, the MEAM model predicts that the liquid-phase Gibbs free energy stays lower than the solid-phase Gibbs free energy even at temperatures down to 1000 K, whereas the experimental temperature is around 3000 K. Due to the glass transition, we are not able to obtain the true liquid free energy at temperatures lower than 1000 K. Therefore, we are not able to determine the melting point of the MEAM model for these BCC metals.

Fortunately, the new MEAM model [17, 18] that includes the second nearest neighbor interactions (2NN-MEAM) seems to be much more robust than the original MEAM model. The melting points predicted by 2NN-MEAM fall within 20% of experimental values. The thermal expansion coefficient also becomes much closer to the experimental values. Hence 2NN-MEAM is a better model for BCC metals than the original MEAM model. It is interesting to note that for the 2NN-MEAM model, the angular cut-off parameter $c_{\min}$ is also much smaller than that in the original MEAM model. Therefore, reducing $c_{\min}$ seems to improve the behavior of MEAM models for both FCC and BCC metals.

3. Free energy method for melting point calculation

Because the melting point is defined as the temperature at which Gibbs free energies of the solid and liquid phases are equal to each other, the melting point can be determined if we know the Gibbs free energies of the two phases as functions of temperature accurately in the neighborhood of the melting point. Since the first calculation of the melting point of Si by the free energy method two decades ago [3], several advanced methods have been developed, such as the adiabatic switching (AS) and reversible scaling [4, 5], which has made free energy calculations much more efficient. Using these state-of-the-art methods, we find that the melting points can be obtained to a much higher accuracy (e.g. ± 1 K) than that achievable by the co-existence method. To achieve such a high accuracy, it is important to carefully choose the beginning and end states of the switch, as well as the switching paths, in order to reduce statistical and systematic error in every step of computation. Because many independent free energies need to be computed to determine the melting point, a large error in any of these steps can undermine the overall accuracy.

Our approach to computing the melting point T_{m} of a pure element can be described by the following steps.

(i) Pick a temperature T_{l} lower than the estimated value of T_{m}. Find the equilibrium volume V_{l} of the crystalline solid at T_{l} by an MD simulation under the NPT ensemble.
(ii) Determine the Helmholtz free energy F_{s} of the solid phase at V_{l} and T_{l}. This is done by AS from the solid phase described by the actual potential model to the harmonic

approximation of the same potential function. Since V_1 is the equilibrium volume, i.e. pressure $P = 0$, $F_s(T_1, V_1)$ equals the Gibbs free energy $G_s(T_1)$ at zero pressure.

(iii) Obtain the Gibbs free energy, $G_s(T)$, of the solid phase as a function of temperature using the reversible scaling method in the domain of $T_1 < T < T_2$, where T_2 is expected to be higher than T_m.

(iv) Find the equilibrium volume V_2 of the liquid phase at T_2 by an MD simulation under the NPT ensemble.

(v) Determine the Helmholtz free energy F_L of the liquid phase at V_2 and T_2. This is done by AS from the liquid to a purely repulsive potential and then to the ideal gas limit. Again $F_L(T_2, V_2)$ equals the Gibbs free energy $G_L(T_2)$ at zero pressure.

(vi) Obtain the Gibbs free energy of the liquid phase as a function of temperature using the reversible scaling method, $G_L(T)$, in the domain of $T_1 < T < T_2$.

(vii) Plot $G_S(T)$ and $G_L(T)$ together and determine the melting temperature at which the two curves cross.

All simulations are performed by molecular dynamics under periodic boundary conditions in three directions and with a time step of $\Delta t = 0.1$ fs. Every switching simulation has the duration of 100 ps unless otherwise mentioned. Si and Ge are modeled using a supercell with 512 atoms that is $5 \times 5 \times 5$ times of a diamond-cubic unit cell. Au, Cu, Ag, and Pb are modeled using a supercell with 500 atoms that is $4 \times 4 \times 4$ times of an FCC unit cell. Mo, Ta and W are modeled using a supercell with 432 atoms that is $6 \times 6 \times 6$ times of a BCC unit cell.

The most challenging part of this work is probably to correctly assemble the results from many different kinds of calculations. Fortunately, this has been automated in the MD++ program in the form of an input script file [7]. In the following, we describe the important details for the different steps of our calculations.

3.1. Solid free energy

The Helmholtz free energy F of a system of N atoms that can be described by a Hamiltonian $H(\{\boldsymbol{r}_i, \boldsymbol{p}_i\})$ is defined by the partition function Z,

$$e^{-\beta F} = Z = \frac{1}{N! h^{3N}} \int \prod_{i=1}^{N} d\boldsymbol{r}_i d\boldsymbol{p}_i e^{-\beta H(\{\boldsymbol{r}_i, \boldsymbol{p}_i\})} \tag{1}$$

where h is Planck's constant, $\beta = 1/(k_B T)$, T is temperature and k_B is Boltzmann's constant. Free energy is difficult to calculate because it cannot be expressed as an ensemble average, such as total energy, which can then be computed by MD or MC simulations as a time average. On the other hand, the free energy difference between two systems can be expressed in terms of an average. Hence, free energy can be computed from the difference between the free energy of the system of interest and that of a reference system whose free energy is known *a priori*. The computation is most efficient when the reference system is very similar to the original system of interest [22].

A widely used reference system is the Einstein crystal, in which every atom is represented by an independent harmonic oscillator vibrating around its perfect lattice positions [24]. However, a reference system that is even closer to the original system is the harmonic approximation of the interatomic potential itself. In this work, we use the quasi-harmonic-approximation (QHA) as the reference system, whose potential function is the Taylor expansion of the original potential function up to second order around the equilibrium lattice positions at the given temperature T_1 (i.e. allowing thermal expansion). The free energy of the reference system is obtained by first computing the Hessian matrix, which is the second derivatives of

the potential energy function with respect to atomic coordinates, and diagonalizing it. Let Λ_i be the eigenvalues of the Hessian matrix. The eigenfrequencies of the normal modes of the crystal are $\omega_i = \sqrt{\Lambda_i/m}$, where m is the atomic mass. The Helmholtz free energy of the reference system is

$$F_{\mathrm{QHA}}(N, V_1, T_1) = E_0(V_1) - k_{\mathrm{B}}T_1 \sum_i \ln \frac{k_{\mathrm{B}}T_1}{\hbar w_i(V_1)}, \tag{2}$$

where $\hbar \equiv h/(2\pi)$.

The Helmholtz free energy difference between the QHA reference system and the real potential at T_1 and V_1 is computed by the AS method [4]. Suppose H_1 is the Hamiltonian of the system of interest and H_0 is the reference system. We define a new Hamiltonian parametrized by λ,

$$H(\lambda) = (1-\lambda)H_0 + \lambda H_1 \tag{3}$$

such that $H(\lambda = 0) = H_0$ and $H(\lambda = 1) = H_1$. During the AS simulation, λ gradually changes from 0 to 1, and the Hamiltonian gradually changes from the reference system to the system of interest. The work done during the switching, ΔW, provides an estimator to the free energy difference, i.e.

$$F_1 - F_0 = \Delta W \equiv \int_0^{t_{\mathrm{sw}}} \frac{\partial H(\lambda)}{\partial \lambda} \frac{\mathrm{d}\lambda(t)}{\mathrm{d}t}\,\mathrm{d}t, \tag{4}$$

where t_{sw} is the total time of the switching simulation. Strictly speaking, the equality $(F_1 - F_0 = \Delta W)$ is valid only in the limit of infinitely slow switching, i.e. $t_{\mathrm{sw}} \to \infty$. For any switching performed at a finite rate, ΔW contains both statistical and systematic error. The systematic error is caused by dissipation in an irreversible process, which makes the averaged work over many independent switching trajectories, $\langle \Delta W \rangle$, greater than $F_1 - F_0$ [23]. To reduce statistical error generated from finite switching time, we employed the switching function

$$\lambda(t) = s^5(70s^4 - 315s^3 + 540s^2 - 420s + 126), \tag{5}$$

where $s = t/t_{\mathrm{sw}}$. This switching function makes the increase rate of λ very low both at the beginning and at the end of the switching trajectory where the fluctuation $\partial H(\lambda)/\partial\lambda = H_1 - H_0$ tends to be largest [22]. The switching function is also very smooth, which was found to be important for error reduction [4].

The following details are important for the calculations of Helmholtz free energy of the solid phase at a given temperature.

(i) There are always three zero eigenfrequencies corresponding to the three rigid-translational modes. This means that the sum over i in equation (2) should include $3(N-1)$ terms. To be self-consistent, similar considerations are needed in the calculation of the free energy of the ideal gas reference system (see next section).
(ii) The Nose–Hoover chain method [25] is needed in the MD simulation to ensure ergodicity since the Hamiltonian is very close to that of a harmonic system.
(iii) Reverse switching simulations are required to estimate and cancel the dissipation [22]. Prior to each switching simulation, it is important to equilibrate the system for a long enough time.

Since the solid is under zero pressure at T_1 and V_1, the Helmholtz free energy $F_{\mathrm{s}}(T_1, V_1)$ is also the Gibbs free energy $G_{\mathrm{S}}(T_1)$ at pressure $P = 0$. In the following, we will omit P in the Gibbs free energy expression, since the latter is always evaluated at zero pressure in this work. The reversible scaling method is used to compute the Gibbs free energy as a

function of temperature [5]. The key idea is to multiply the potential energy function U by a parameter $\lambda(t)$, which changes smoothly with time t during the switching simulation. The simulation is performed at a constant temperature T_0. But the work done to the system during the switching simulation can be used to extract the free energy of the original system (with potential function U) in a range of temperatures $T = T_0/\lambda(t)$. The following details are important for a successful calculation.

(i) The NPT ensemble is required to ensure zero pressure during the switch simulation.
(ii) The Nose–Hoover chain method is required to ensure ergodicity.
(iii) Reverse switching should be performed to estimate and cancel the dissipation.
(iv) The range of $\lambda(t)$ should be limited to avoid large dissipation. This means that if the initial guess T_1 is too far away from the predicted melting point T_m, we need to repeat the previous step (compute solid free energy with QHA) at a different temperature T_1 that is closer to T_m, in order to reduce the error bar.

3.2. Liquid free energy

The ideal gas is used as the reference system to compute the Helmholtz free energy of the liquid phase at temperature T_2 and volume V_2. The Helmholtz free energy of N ideal gas particles is

$$F_{\text{i.g.}}(N, V_2, T_2) = -k_B T_2\{N \ln(V_2/\Lambda^3) - \ln N!\}, \tag{6}$$

where V_2 is the equilibrium volume of liquid at T_2 and $\Lambda \equiv h/\sqrt{2\pi m k_B T}$ is the thermal de Broglie wave length. It is important to point out that we need to replace N by $N - 1$ when using the above equation to compute the free energy of the reference system, due to the fixed center of mass in atomistic simulations (see previous section).

To minimize dissipation which causes a systematic error in the switching simulation, we should always avoid crossing any phase transition line during the AS. It is generally expected that a direct switching path from a liquid phase to an ideal gas will cross the liquid–gas transition line. To avoid this, we first switch the liquid to an intermediate reference system and then switch to the ideal gas limit. The intermediate reference system is a collection of N particles interacting through a purely repulsive pair potential of the following Gaussian form

$$\phi(\boldsymbol{r}_i, \boldsymbol{r}_j) = \lambda\epsilon \exp\left(\frac{-|\boldsymbol{r}_i - \boldsymbol{r}_j|}{2\sigma}\right). \tag{7}$$

ϵ and σ are adjusted to minimize dissipation occurring when switching to and from the real potential model.

We find that the Gaussian potential is a better reference system than the inverse-12 potential (i.e. $1/r^{12}$) used in the literature [26]. Even though the free energy of the inverse-12 potential is available in analytic form as a Virial expansion, the expansion may not converge within 10 terms at the density of the silicon liquid. While the free energy of the Gaussian potential liquid is not known analytically, it can be easily computed by AS to the ideal gas limit. Because the Gaussian potential is very simple, the computational cost required in this step is negligible compared with other steps where the real potential model (e.g. SW, MEAM) is required. This enables us to break the switching path into many smaller steps, reducing the systematic error caused by the large difference between the beginning and the end states. The lack of singularity of the Gaussian potential (in contrast to the inverse-12 potential) also improves the numerical convergence. Because we never observe a large dissipation (i.e. the total work in the forward and reverse switching) in our simulations, this can be taken as an empirical proof that we did not cross any phase-transition line along the switching path.

The following details are important for the calculations of Helmholtz free energy of the liquid phase at a given temperature.

(i) Switching from the Gaussian potential to the ideal gas limit must be performed in several steps for accuracy if a linear switching function is used. We multiply the potential energy U by a parameter λ. $\lambda = 1$ is the original fluid with the Gaussian potential and $\lambda = 0$ is the ideal gas limit. In our simulation, we switch from $\lambda = 1$ to $\lambda = 10^{-6}$ in 6 steps, each time reducing λ by a factor of 10. Further reduction of λ produces a negligible amount of work, confirming that the ideal gas limit has been reached.

(ii) To minimize dissipation and statistical error, we should adjust the parameters of the Gaussian potential to match the characteristic distance and energy scale of the real potential. For example, σ and ϵ can be adjusted to mimic the pair potential part of the SW potential. ϵ of 50 eV and σ of 0.7 Å are used with cut-off length $r_c = 3.771$ Å for the case.

(iii) Reverse switching must be performed to estimate and correct for dissipation.

Since the liquid is under zero pressure at temperature T_2 and volume V_2, the Helmholtz free energy $F_L(T_2, V_2)$ is also the Gibbs free energy $G_L(T_2)$. The Gibbs free energy of the liquid phase as a function of temperature is then obtained using the same reversible scaling method as in the previous section. The Nose–Hoover chain method is no longer needed for the simulation in the liquid phase because the system is far away from being harmonic and ergodicity is satisfied.

3.3. Melting point and error estimate

After obtaining the Gibbs free energies of both the solid and the liquid phases, $G_S(T)$ and $G_L(T)$, in the temperature range of $T_1 < T < T_2$, we fit both data into smooth spline functions and determine the point at which the two functions cross each other. The temperature at which the two functions cross is the melting point T_m.

The error bar on T_m is computed from the errors in the free energy estimates in the switching simulations. Each switching simulation S_i (e.g. switching between two Hamiltonians or switching along the temperature axis) is repeated n ($\sim$10) times, which results in n independent values of the irreversible work ΔW. Given these works in both forward and reverse directions, the free energy difference between the two systems is estimated using an extension of Bennett's acceptance ratio method [27, 28]. This estimator was shown to be unbiased (i.e. with zero systematic error) and to have the smallest statistical error. The free energy difference ΔF_i is obtained by solving the following equations self-consistently:

$$e^{-\beta \Delta F_i} = \frac{\langle (1 + e^{\beta \Delta W_i + C})^{-1} \rangle_F}{\langle (1 + e^{\beta \Delta W_i - C})^{-1} \rangle_R} e^C \tag{8}$$

$$C = -\beta \Delta F_i + \ln n_F / n_R \tag{9}$$

where n_F and n_R are the number of independent forward and reverse switching simulations [27, 28]. This expression is exact even for very rapid switching trajectories where linear response theory is no longer valid. The standard deviation σ_i of the estimated ΔF_i can be obtained from the following equation:

$$\beta^2 \hat{\sigma}_i^2 = \frac{\mathrm{Var}[(1 + e^{\beta W_i + C})^{-1}]_F}{n_F \langle (1 + e^{\beta W_i + C})^{-1} \rangle_F^2} + \frac{\mathrm{Var}[(1 + e^{\beta W_i - C})^{-1}]_R}{n_R \langle (1 + e^{\beta W_i - C})^{-1} \rangle_R^2}, \tag{10}$$

where $\mathrm{Var}[x]$ is the variance of the random variable x.

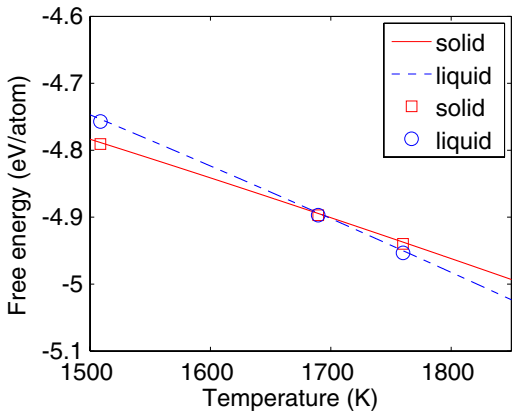

Figure 1. Gibb's free energy per atom for both the solid phase (solid line) and liquid phase (dashed line). The symbols represent data points in Broughton and Li [3] with squares for the solid phase and circles for the liquid phase.

(This figure is in colour only in the electronic version)

In this work, the melting point is estimated from $m = 5$ different types of switching simulations. Assuming the error made in each switching simulation is independent of each other, the error bar for the Gibbs's free energy difference between the solid and the liquid phases is estimated by

$$\sigma(\Delta G) = \left(\sum_{i=1}^{m} (\hat{\sigma}_i)^2 \right)^{1/2}. \tag{11}$$

The error bar in the melting point prediction is

$$\sigma(T_{\mathrm{m}}) = \frac{\sigma(\Delta G)}{S_{\mathrm{L}} - S_{\mathrm{S}}}, \tag{12}$$

where S_{L} and S_{S} are the entropy of the liquid and solid phases at the melting point, respectively. The entropies can be obtained from the slope of the Gibbs free energy–temperature curve.

An example is given in figure 1, which plots the Gibbs free energy as a function of temperature for the liquid and solid phases of Si, as described by the SW potential. The dominant source of error comes from the switching simulation between the SW liquid to the Gaussian fluid (see appendix A for more details). This error contributes to an uncertainty of 0.884×10^{-4} eV atom^{-1} in the liquid Gibbs free energy, which corresponds to melting temperature uncertainty of 0.46 K. Semiconductors and FCC metals studied here show similar error bars. The error bars of BCC metals are considerably higher, most likely due to their high melting temperature, which leads to larger statistical fluctuation.

Repeating each AS simulation for $n = 20$ times usually brings the error bar of the melting point to within ± 1 K. The accuracy of this level can be readily achieved in a day using a computer cluster with 30 CPUs. Due to limited computational resources, enough computation is performed to reach ± 1 K accuracy only for MEAM-Si, SW-Si and MEAM-Au models. For other models, each AS simulation is performed only 5 or 6 times, leading to a larger error bar in the predicted free energy. The finite size of the simulation cell and small uncertainty in the determination of the equilibrium volume at finite temperature can introduce additional error to the melting point, which is not accounted for in our error estimate.

Table A1. The estimated free energy difference ΔF_i and its standard deviation in the five different AS steps for the melting point calculations of SW-Si and MEAM-Si models.

	SW-Si		MEAM-Si	
i	ΔF_i (eV atom^{-1})	$\hat{\sigma}_i$ (10^{-4} eV atom^{-1})	ΔF_i (eV atom^{-1})	$\hat{\sigma}_i$ (10^{-4} eV atom^{-1})
1	−0.012 97	0.01	−0.006 24	0.07
2	0.816 16	0.05	1.105 44	0.03
3	−3.687 33	0.88	−3.940 27	1.01
4	0.500 80	0.45	0.410 05	0.47
5	−1.138 76	0.19	−1.213 68	0.26

4. Summary

We have computed the melting points, latent heat, entropy and thermal expansion coefficients for nine pure elements described by four different interatomic potential models. The state-of-the-art free energy methods are used to determine the melting points accurately and efficiently, allowing a systematic comparison between the potential models. The beginning and end states and the switching paths are chosen carefully in the AS simulations to reduce the error in the free energy calculation. The comparison reveals several systematic trends among elements with the same crystal structure. The MEAM model performs reasonably well in semiconductors compared with the SW model, and predicts more accurate thermal properties than the EAM model, especially the angular screening factor is adjusted. The original MEAM model fails to predict reasonable thermodynamic properties for BCC metals. In comparison, the FS model and the 2NN-MEAM model are more reliable for BCC metals.

Acknowledgments

We would like to thank Dr M Baskes, Dr A Caro and Dr G A Galli for useful discussions. This work is partly supported by the DOE/SciDAC project on Quantum Simulation of Materials and Nanostructures and NSF/CMMI Nano Bio Materials Program CMS-0556032. SR acknowledges support from the Stanford Graduate Fellowship Program.

Appendix A. Error estimates in free energy calculations

In this appendix, we present some intermediate free energy results of our melting point calculations. The purpose is two-fold. First, it will enable interested readers to compare their results with ours, should they wish to adopt our computational method. Second, it demonstrates which step is the major source of error in the final estimate of the melting point. This allows further improvement of the accuracy and efficiency of melting point calculations in the future. The average and standard deviation of the reversible work accumulated in each of the five AS steps (counting forward and backward switching together) are listed in table A1.

Step 1 corresponds to AS from a solid phase described by an empirical potential to the QHA of itself. Step 2 corresponds to switching the solid phase along the temperature axis from T_1 to T_1/λ_1. $T_1 = 1600$ and $\lambda_1 = 0.8$ are used for SW Si and $T_1 = 1200$ and $\lambda_1 = 0.75$ are used for MEAM Si. Step 3 corresponds to AS from a liquid phase described by an empirical potential to the purely repulsive liquid described by the Gaussian potential. Step 4 corresponds to AS from the Gaussian potential to the ideal gas limit. Step 5 corresponds to switching the liquid phase along the temperature axis from T_2 to T_2/λ_2. $T_2 = 1800$ and $\lambda_2 = 1.3$ are used

for SW Si and $T_2 = 1560$ and $\lambda_2 = 1.3$ are used for MEAM Si. Table A1 shows that the intermediate results are similar for the SW-Si and the MEAM-Si models, both in terms of the average free energy differences and in terms of the error bars. The major source of error comes from the switching between the liquid phase and the purely repulsive liquid described by the Gaussian potential (step 3).

References

[1] Cook S J and Clancy P 1993 *Phys. Rev.* B **47** 7686
[2] Landman U *et al* 1986 *Phys. Rev. Lett.* **56** 155
[3] Broughton J Q and Li X P 1987 *Phys. Rev.* B **35** 9120
[4] Watanabe M and Reinhardt W P 1990 *Phys. Rev. Lett.* **65** 3301
[5] de Koning M, Antonelli A and Yip S 1999 *Phys. Rev. Lett.* **83** 3973
[6] Kaczmarski M, Rurali R and Hernández E 2004 *Phys. Rev.* B **69** 214105
[7] MD++ source codes and automatic scripts for free energy and melting point calculations can be downloaded at http://micro.stanford.edu/∼caiwei/Forum
[8] Stillinger F H and Weber T A 1985 *Phys. Rev.* B **31** 5262
[9] Ding K and Andersen H C 1986 *Phys. Rev.* B **34** 6987
[10] Park H S and Zimmerman J A 2005 *Phys. Rev.* B **72** 054106
[11] Aubry S and Hughes D A 2006 *Phys. Rev.* B **73** 224116
[12] Finnis M W and Sinclair J E 1984 *Phil. Mag.* A **50** 45
[13] Baskes M I 1992 *Phys. Rev.* B **46** 2727
[14] Lide D R 2007-2008 *CRC Handbook of Chemistry and Physics* 88th edn (New York: CRC Press)
[15] Chase M W Jr 1998 *NIST-JANAF Thermochemical Tables* 4th edn (Washington, DC: AIP)
[16] Hirth H P and Loath J 1982 *Theory of Dislocations* 2nd edn (Malabar, FL: Krieger)
[17] Lee B J and Baskes M I 2000 *Phys. Rev.* B **62** 8564
[18] Lee B J, Baskes M I, Kim H and Cho Y K 2001 *Phys. Rev.* B **64** 184102
[19] Baskes M I, Nelson J S and Wright A F 1989 *Phys. Rev.* B **40** 6085
[20] Baskes M I 2008 personal communications
[21] Cai W, Weinberger C R and Baskes M I 2008 unpublished
[22] Bulatov V V and Cai W 2006 *Computer Simulations of Dislocations* (Oxford: Oxford University Press)
[23] Jarzynski C 1997 *Phys. Rev. Lett.* **78** 2690
[24] de Koning M and Antonelli A 1996 *Phys. Rev.* E **53** 465
[25] Martyna G J and Klein M L 1992 *J. Chem. Phys.* **97** 15
[26] Young D A and Rogers F J 1984 *J. Chem. Phys.* **80** 2789
[27] Crooks G E 2000 *Phys. Rev.* E **61** 2361
[28] Bennett C H 1976 *J. Comput. Phys.* **22** 245